Journal of Applied Physics

RESEARCH ARTICLE | FEBRUARY 26 2025

Pressure-regulated bandgap narrowing and photoelectric activity enhancement in layered halide compound GeI_2

Zhongyang Li ; Yiming Wang ; Xiaohui Zeng ; Shuo Zhou; Zhikai Zhu; Kai Zhang; Kejun Bu ; Chengxuan Song ; Haiyun Shu; Shuai Yan; Dongbo Wang ; Wenge Yang ; Gang Liu; Yanfeng Guo ; Lingping Kong

J. Appl. Phys. 137, 085902 (2025)
https://doi.org/10.1063/5.0256512

Journal of Applied Physics ARTICLE pubs.aip.org/aip/jap

Pressure-regulated bandgap narrowing and photoelectric activity enhancement in layered halide compound GeI_2

Cite as: J. Appl. Phys. **137**, 085902 (2025); doi: 10.1063/5.0256512
Submitted: 5 January 2025 · Accepted: 12 February 2025 ·
Published Online: 26 February 2025

Zhongyang Li,[1,2] Yiming Wang,[2] Xiaohui Zeng,[1] Shuo Zhou,[2,3] Zhikai Zhu,[2] Kai Zhang,[2] Kejun Bu,[2] Chengxuan Song,[1] Haiyun Shu,[2] Shuai Yan,[4] Dongbo Wang,[3] Wenge Yang,[2,a)] Gang Liu,[2,5] Yanfeng Guo,[1,6,a)] and Lingping Kong[2,a)]

AFFILIATIONS

[1]School of Physical Science and Technology, ShanghaiTech University, Shanghai 201210, China
[2]Center for High Pressure Science and Technology Advanced Research, Shanghai 201203, China
[3]School of Materials Science and Engineering, Harbin Institute of Technology, Harbin 150001, China
[4]Shanghai Advanced Research Institute, Chinese Academy of Sciences, Shanghai 201204, China
[5]Shanghai Key Laboratory of Material Frontiers Research in Extreme Environments (MFree), Shanghai Advanced Research in Physical Sciences (SHARPS), Shanghai 201203, China
[6]ShanghaiTech Laboratory for Topological Physics, ShanghaiTech University, Shanghai 201210, China

[a)]**Authors to whom correspondence should be addressed:** yangwg@hpstar.ac.cn; guoyf@shanghaitech.edu.cn; and konglp@hpstar.ac.cn

ABSTRACT

Layered semiconductors offer distinct advantages for optoelectronically responsive heterojunction devices due to their strong light–matter interactions and weak interlayer van der Waals interactions, which enable exfoliation into adjustable thicknesses. However, their practical utility is often restricted by excessively wide bandgaps, which limit spectral response within the visible light range and reduce light absorption efficiency, thereby constraining broadband detection capabilities. In this study, pressure was employed as a tuning parameter to modulate the bandgap and optimize the photoelectric performance of the layered semiconductor GeI_2. Structural stability under moderate compression (5 GPa) was confirmed through *in situ* Raman spectra and x-ray diffraction, with no evidence of phase transition. At 5 GPa, a remarkable five-order-of-magnitude enhancement in photoelectric activity was observed. *In situ* UV-visible absorption spectroscopy, supported by theoretical calculations, revealed that this enhancement is primarily driven by pressure-induced narrowing of the bandgap. These findings offer critical insights for designing two-dimensional broadband photodetectors with tailored bandgap properties and enhanced photoelectric response, contributing to advancing next-generation flexible optoelectronic devices.

I. INTRODUCTION

Photodetectors, which convert electromagnetic optical signals into electrical signals, are essential components in various technological applications. With the rapid advancement of optoelectronic technologies, the demand for high-performance broadband photodetection materials has grown significantly to meet the needs of critical applications such as optical communications,[1] imaging systems,[2] and sensing technologies.[3,4] Traditional photodetection materials, including silicon and III–V semiconductors, have played a pivotal role in the field due to their excellent electronic properties, scalability, and well-established fabrication techniques. Despite their success, silicon-based photodetectors face limitations in their narrow spectral response range and rigid form factor, while III–V semiconductors are constrained by high production costs.[5–7] To overcome these limitations, recent research has focused on the development of novel materials with

superior optoelectronic properties, such as broad spectral absorption,[8,9] high responsivity,[10] and rapid response times.[11]

Two-dimensional (2D) materials have emerged as up-and-coming candidates for photoelectric detection, primarily due to their distinctive properties, including strong light–matter interactions, tunable thicknesses through adjustable layer numbers, and layer-dependent electronic structures.[12,13] Materials such as graphene, transition metal dichalcogenides (TMDs), and black phosphorus have demonstrated exceptional performance across a broad spectral range, from ultraviolet to infrared.[14–18] The atomically thin nature of 2D materials further enables the fabrication of flexible and transparent photodetectors, which are particularly advantageous for applications in wearable electronics and transparent optoelectronic devices.[13] Beyond conventional photodetection, 2D materials exhibit significant potential in self-powered optoelectronic systems.[19,20] For instance, field-effect transistors based on exfoliated van der Waals (vdW) semiconductor SnP_2Se_6 flakes demonstrate excellent optoelectronic performance, including rapid photoresponse times ($\approx 3\,\mu s$) and high detectivity values ($>10^{14}$ Jones), highlighting their suitability for advanced electronic and optoelectronic applications.[21] Additionally, layered ferroelectric materials, such as $CuInP_2S_6$, have shown a remarkably enhanced bulk photovoltaic effect, achieving photocurrent densities that are two orders of magnitude higher than traditional ferroelectric perovskite oxides. This enhancement, driven by room-temperature polar ordering, positions $CuInP_2S_6$ as a highly efficient candidate for ultrathin third-generation photovoltaic technologies.[22]

External pressure provides a powerful approach for directly compressing chemical bonds, enabling precise tuning of the crystal and electronic structures of materials.[23] This method has proven highly effective in optimizing material properties for advanced technological applications. Recent advancements have demonstrated the effectiveness of applying pressure to modify the crystal and electronic structures of hybrid iodide perovskite systems. These soft-lattice materials, renowned for their structural tunability, have shown significant potential for optimizing bandgap and luminescence properties through pressure effect.[24,25] In the all-inorganic 2D halide perovskite $Cs_2PbI_2Cl_2$, the application of pressure has been shown to enhance exciton binding energy, resulting in a substantial increase in photocurrent.[26] Similarly, pressure has been utilized to improve photocurrent performance and expand detection bandwidths in binary halide systems such as CsI_3 and PbI_2.[27,28] In the case of the 2D noble metal halide semiconductor RhI_3, pressure-induced effects are particularly striking, including bandgap narrowing, increased carrier concentration, enhanced photocurrent, and even metallization at higher pressures.[29] These findings underscore the versatility of pressure as an innovative tool for engineering material properties. By exploiting pressure-induced modifications, researchers can design and develop broadband optoelectronic devices tailored to meet the demands of next-generation technologies, opening new avenues for functional material advancements.

Among various 2D materials, germanium diiodide (GeI_2) has emerged as a highly promising 2D material due to its unique properties, including a layered crystal structure that allows for the production of atomically thin, stable flakes through cost-effective mechanical exfoliation. These attributes make GeI_2 an excellent candidate for fabricating high-performance photodetectors with reduced dimensionality.[30] Moreover, its non-toxic nature positions GeI_2 as an environmentally friendly alternative to lead-based compounds, addressing safety and environmental concerns associated with hazardous materials in optoelectronics. In this study, we systematically explored the structural and physical properties of GeI_2 under both ambient and high-pressure conditions. Using *in situ* characterization techniques, including Raman spectra, UV-visible absorption spectroscopy, and synchrotron-based powder x-ray diffraction (XRD), we investigated the fundamental behavior of GeI_2 and its potential for photoelectric detection applications. Additionally, we analyzed the pressure-induced modulation of its electronic structure and photoelectric response, offering valuable insights into its behavior under varying external conditions. Our findings provide a foundation for the design and optimization of photodetectors built upon this promising 2D material.

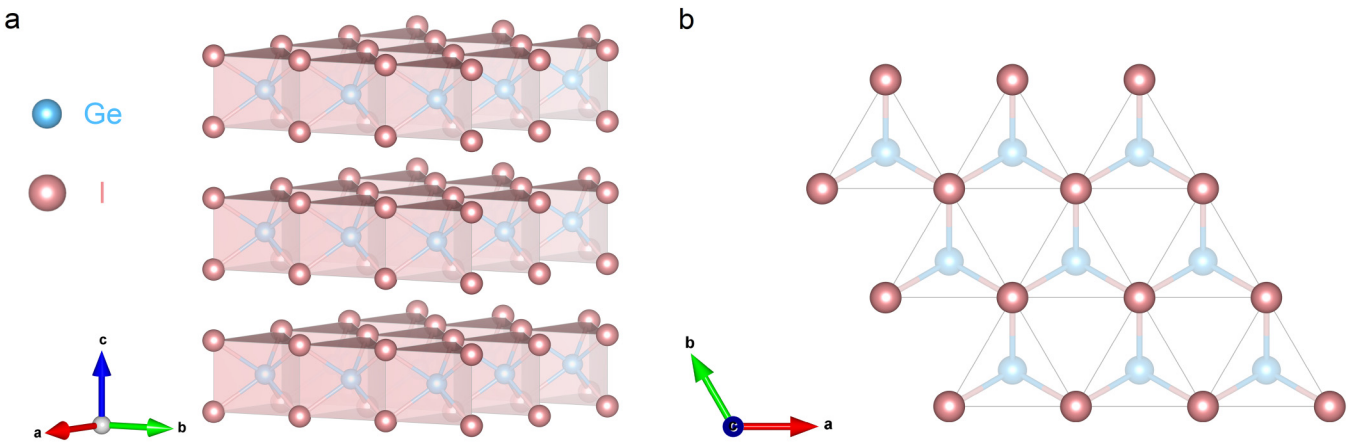

FIG. 1. (a) and (b) Schematic representations of the GeI_2 crystal structure from multiple perspectives.

II. RESULTS AND DISCUSSION

Millimeter-scale, yellow GeI_2 crystals with a layered structure were synthesized using a chemical vapor transport (CVT) method. The synthesis process involved combining Ge powder (99.999%, Macklin) and iodine spheres (99.99%, Macklin) in a stoichiometric ratio of Ge: I = 1:1, followed by sealing the mixture in a quartz tube under a vacuum pressure lower than 1 Pa to ensure a clean reaction environment. This reduced iodine ratio, compared to the material stoichiometry of Ge: I = 1:2, successfully prevented the formation of impurity phase GeI_4. The quartz tube was hermetically sealed and placed horizontally in a single-temperature zone tube furnace, with raw materials positioned at the cooler end and crystallization of GeI_2 occurring at the hotter end, which was maintained at 440 °C. After 1 week of reaction, the furnace was allowed to be cooled to room temperature in air. This process yielded high-quality, layered GeI_2 crystals.

To check the crystal morphology and composition of as-prepared GeI_2 crystals, scanning electron microscopy (SEM) and energy dispersive x-ray spectroscopy (EDS) measurements were performed. As shown in Figure S2(a) in the supplementary material, the 2D characteristics of the GeI_2 crystal are visible. The EDS spectroscopy in Figure S2(b) in the supplementary material displays the characteristic peaks of Ge and I elements, and further analysis indicates an elemental ratio of Ge:I at 1:1.94, which is close to the ideal stoichiometry. Additionally, EDS mapping measurements [Figure S2(c) in the supplementary material] reveal

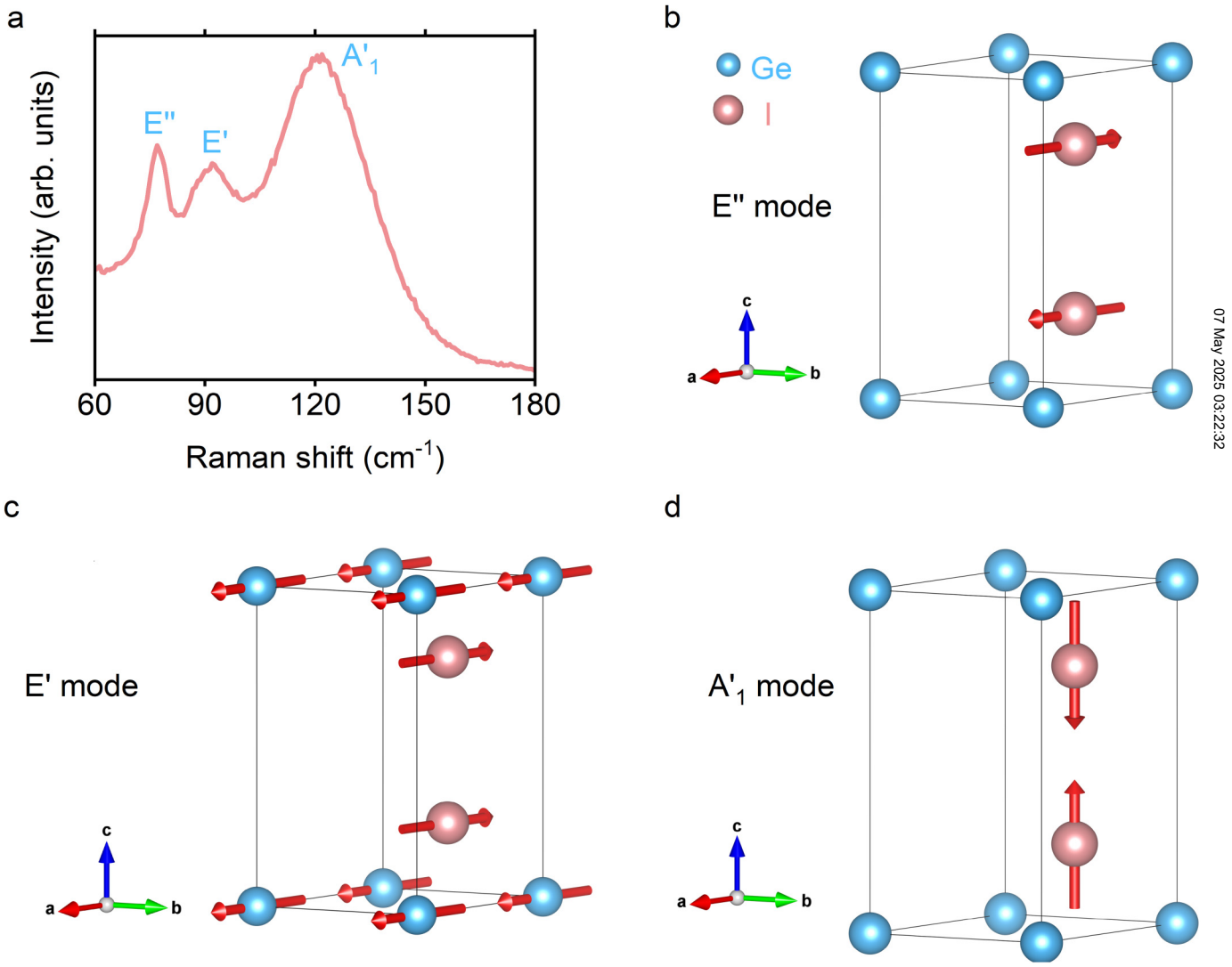

FIG. 2. (a) Raman spectrum of GeI_2. (b)–(d) The calculated frequencies of Raman-active vibration modes of GeI_2.

that the elements in areas of uniform thickness are evenly distributed. Crystals with varying thicknesses exhibited different contrasts due to differences in focus.

The crystal structure of GeI_2 belongs to the $P\bar{6}m2$ space group and is composed of [GeI_6] triangular prisms arranged in the *ab* plane, sharing edges to form a layered structure [Figs. 1(a) and 1(b)].[30] These triangular prisms are perfectly aligned along the *c* axis, with the layers held together by vdW interactions. This vdW-bonded structure facilitates the exfoliation of GeI_2 into atomically thin 2D layers with tunable thicknesses, a property that is particularly advantageous for the fabrication of flexible optoelectronic devices and 2D heterojunctions. Beyond its structural characteristics, GeI_2 possesses inherent thermodynamic stability and non-toxicity, making it a promising alternative to lead-based compounds. Its environmentally friendly nature further enhances its potential for use in next-generation optoelectronic applications. The combination of facile exfoliation, stable layered structure, and non-toxic composition underscores the suitability of GeI_2 for flexible and sustainable device development.

To gain an initial understanding of the crystal structure of GeI_2 under ambient conditions, we analyzed its Raman-active vibrational modes. The Raman spectrum [Fig. 2(a)] shows good

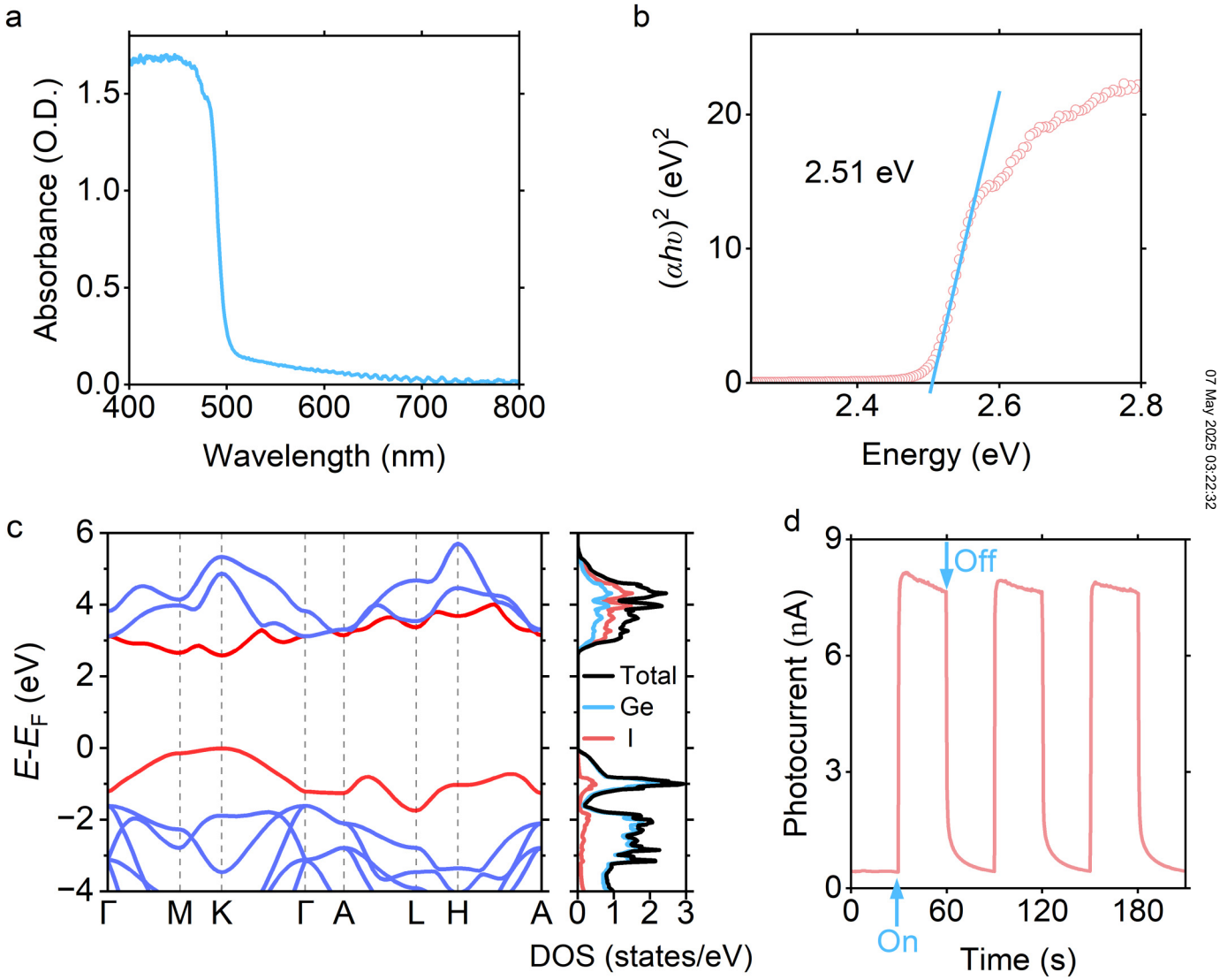

FIG. 3. (a) UV-visible absorption spectroscopy of GeI_2, where the unit of absorbance, O.D. is the abbreviation of optical density. (b) Tauc plot for direct bandgap fitting. (c) The calculated band structure and density of states (DOS) of GeI_2 at ambient conditions, where the conduction band and valence band are highlighted in red. (d) The time-resolved photoelectric response of GeI_2 at ambient conditions was measured over three cycles.

agreement with both theoretical calculations and experimental results reported in previous studies.[30] Specifically, two prominent peaks at 77 and 92 cm^{-1} correspond to the bending vibrational modes of Ge–I bonds, named E″ and E′, respectively, which can be expressed as the interactions within the layer. Additionally, a higher energy peak at 120 cm^{-1} is attributed to the stretching vibrational A_1' mode of I–I bonds, reflecting the interlayer interactions. The schematic diagrams of these vibrational modes are summarized in Figs. 2(b)–2(d). The absence of additional peaks confirms that no impurity phases, such as GeI_4, were formed during synthesis.

Experimentally, the bandgap was determined using UV-visible absorption spectroscopy [Fig. 3(a)]. The absorption spectroscopy exhibits a clear onset near 500 nm, and a Tauc plot analysis for direct bandgap semiconductors yields a bandgap of 2.51 eV [Fig. 3(b)]. To further investigate the electronic properties of GeI_2, density functional theory (DFT) calculations were performed with hybrid functional and vdW corrections taking into consideration [Fig. 3(c)]. More computational details can be found in supplementary materials. To assess the influence of different dispersion correction methods, we also tested vdW-DF, optB88-vdW, Tkatchenko-Scheffler, and DFT-ulg methods, as shown in Figure S2 in the supplementary material. In these calculations, the lattice parameters were fixed to match experimental refinements, while the atomic positions were fully relaxed using each method. Notably, the resulting dispersions were nearly degenerate, demonstrating the feasibility and robustness of the DFT-D3 method we selected. The calculations established that GeI_2 is a direct bandgap semiconductor, characterized by both the conduction band minimum (CBM) and valence band maximum (VBM) residing at the *K* point of the Brillouin zone. The valence band is primarily derived from Ge states, while the conduction band exhibits a hybridized character involving contributions from both Ge and I. Notably, Van Hove Singularities (vHS) emerge at the *H* point of the valence band, characterized by the saddle point in the band structure and a striking peak in the density of states (DOS). The substantial DOS near the Fermi level significantly enhances the likelihood of quantum transitions, laying the foundation for the good optoelectronic performance of GeI_2. The calculated bandgap of GeI_2 is 2.6 eV at ambient pressure, in good agreement with the UV-visible absorption spectroscopy measurement. This demonstrates the robustness of our calculations and suggests the applicability under high-pressure conditions.

The photoelectric response of bulk GeI_2 was also evaluated under ambient conditions. Using a xenon lamp to simulate visible light and applying a 5 V bias, we conducted three cycles of measurements, as shown in Fig. 3(d). The results indicate a rapid and stable response to visible light, highlighting GeI_2's potential for use in advanced optoelectronic devices, including flexible photodetectors. These findings provide a comprehensive understanding of the structural, optical, and photoelectric properties of GeI_2, paving the way for its application in next-generation flexible optoelectronic technologies.

To investigate the pressure effect on the crystal structure of GeI_2, *in situ* Raman spectra were conducted under pressures up to 5 GPa, as shown in Figs. 4(a) and 4(b). During compression, no new Raman peaks emerged, indicating the absence of pressure-induced phase transitions within this range. Instead, all existing peaks systematically shifted to higher wavenumbers. The monotonic rightward shift of the Raman peak positions, as depicted in Fig. 4(c), reflects the continuous contraction of the crystal lattice under increasing pressure, consistent with the expected behavior of a compressing structure.

The physical properties of crystalline materials are highly sensitive to crystal structures under high pressure. To investigate the variation of the GeI_2 crystal structure under high pressure, we performed *in situ* high-pressure powder XRD measurements using synchrotron radiation. The initial 2D diffraction patterns were converted to 1D profiles using Dioptas software.[31] Structural refinements carried out with GSAS-II software[32] confirmed that all diffraction peaks originated from the ambient-pressure phase and shifted systematically to higher angles, consistent with lattice compression, as shown in Fig. 5(a). No new diffraction peaks were observed across the pressure range, indicating the absence of phase transitions. These results establish a foundation for understanding the pressure-induced modulation of GeI_2's physical properties.

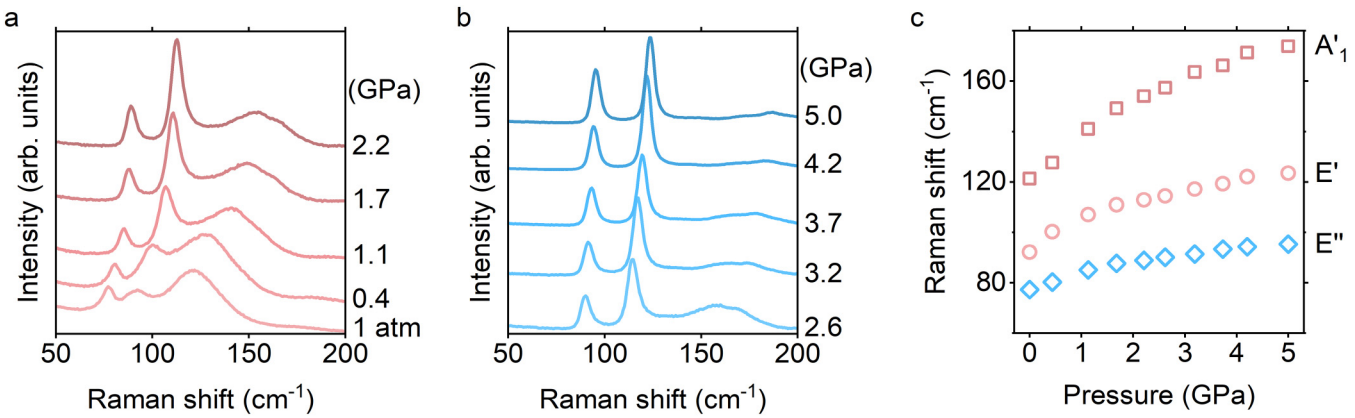

FIG. 4. (a) and (b) Raman spectra under compression. (c) The pressure dependence of Raman peak positions.

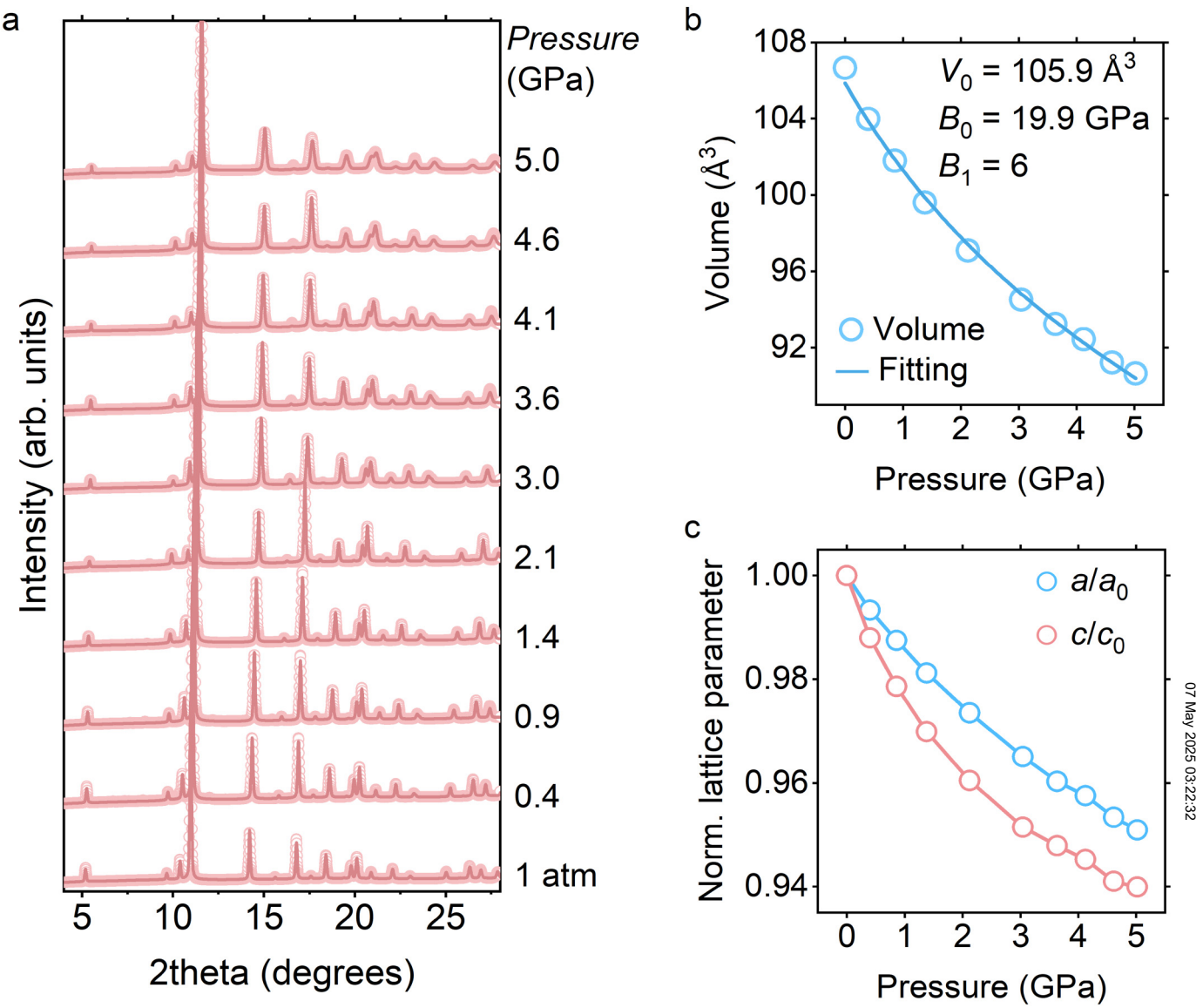

FIG. 5. (a) XRD patterns and refinement under compression. (b) The pressure-dependent evolution of the unit cell volume (V) derived from powder XRD refinements using GSAS-II software. The solid line represents the fit to the EOS. (c) The pressure dependence of normalized lattice parameters (a/a_0 and c/c_0).

The specific lattice parameters, R_{wp}, and *GOF* of refinement at various pressures are shown in Table I.

Structural refinements also provided detailed information on lattice parameters at various pressures, enabling the generation of crystal information files (CIFs) for each compression state. The intra-layer atomic spacing (a), inter-layer spacing (c, which is closely related to the vdW gap), and unit cell volume (V) were tracked as functions of pressure, as presented in Figs. 5(b) and 5(c). Notably, the inter-layer spacing (c) exhibited stronger compression compared to the intra-layer spacing (a), a characteristic behavior observed in other 2D materials.[33–36] This anisotropic compression highlights the dominant role of van der Waals interactions in the structural response to pressure. Furthermore, the evolution of unit cell volume (V) with pressure was fitted using the equation of state (EOS),[37] yielding a bulk modulus of 19.9 GPa. This relatively low bulk modulus confirms that GeI_2 is a mechanically soft 2D semiconductor material. These findings provide a comprehensive understanding of the pressure-dependent structural behavior of GeI_2 and its potential for pressure-tunable electronic and optical properties.

TABLE I. The lattice parameters a and c, lattice volume V of GeI_2, R_{wp}, and GOF of refinement at various pressures.

Pressure (GPa)	a (Å)	c (Å)	V (Å^3)	R_{wp}	GOF
0.0	4.24(4)	6.83(6)	106.65(7)	4.22	1.79
0.4	4.21(6)	6.75(3)	103.98(1)	4.46	2.14
0.9	4.19(1)	6.68(9)	101.76(6)	3.61	1.71
1.4	4.16(4)	6.63(1)	99.59(7)	3.82	1.80
2.1	4.13(2)	6.56(5)	97.08(6)	4.09	1.95
3.0	4.09(6)	6.50(4)	94.51(4)	5.11	2.40
3.6	4.07(5)	6.47(9)	93.23(1)	5.24	2.56
4.1	4.06(4)	6.46(1)	92.43(7)	5.83	2.74
4.6	4.04(6)	6.43(2)	91.22(4)	6.24	2.93
5.0	4.03(6)	6.42(5)	90.65(1)	7.73	3.54

Building on previous studies demonstrating the significant application potential of GeI_2 in low-dimensional semiconductor broadband photodetectors, we performed *in situ* high-pressure photoelectric response measurements on GeI_2 single crystals. These experiments were conducted using a two-electrode configuration within a diamond anvil cell [Fig. 6(a)]. A constant external bias of 5 V was applied, and the sample was illuminated with stable visible light generated by a xenon lamp. The results reveal that the response speed of GeI_2 decreases with increasing pressure, likely due to the higher density of defect states induced by compression. The evolution of photocurrent as a function of pressure is summarized in Fig. 6(b). At ambient pressure, the photocurrent was measured at 0.56 nA, which increased dramatically to 0.04 mA at 5 GPa, representing an enhancement of five orders of magnitude. This remarkable pressure-induced increase highlights the potential for tuning the optoelectronic properties of GeI_2 through external pressure.

In addition to photocurrent measurements, we analyzed the changes in dark current and resistance under compression, as shown in Fig. 6(c). The results indicate a six-order-of-magnitude increase in dark current, accompanied by a corresponding six-order-of-magnitude decrease in resistance with increasing pressure. These trends explain the challenges in measuring photocurrent at pressures beyond 5 GPa, as the high dark current dominates the signal. Overall, these findings provide insights into the pressure-dependent photoelectric behavior of GeI_2, offering valuable guidance for its application in pressure-tunable optoelectronic devices.

The electronic structure of semiconductors, particularly those interacting with visible light, plays a critical role in determining their optical and electronic properties. To further explore the

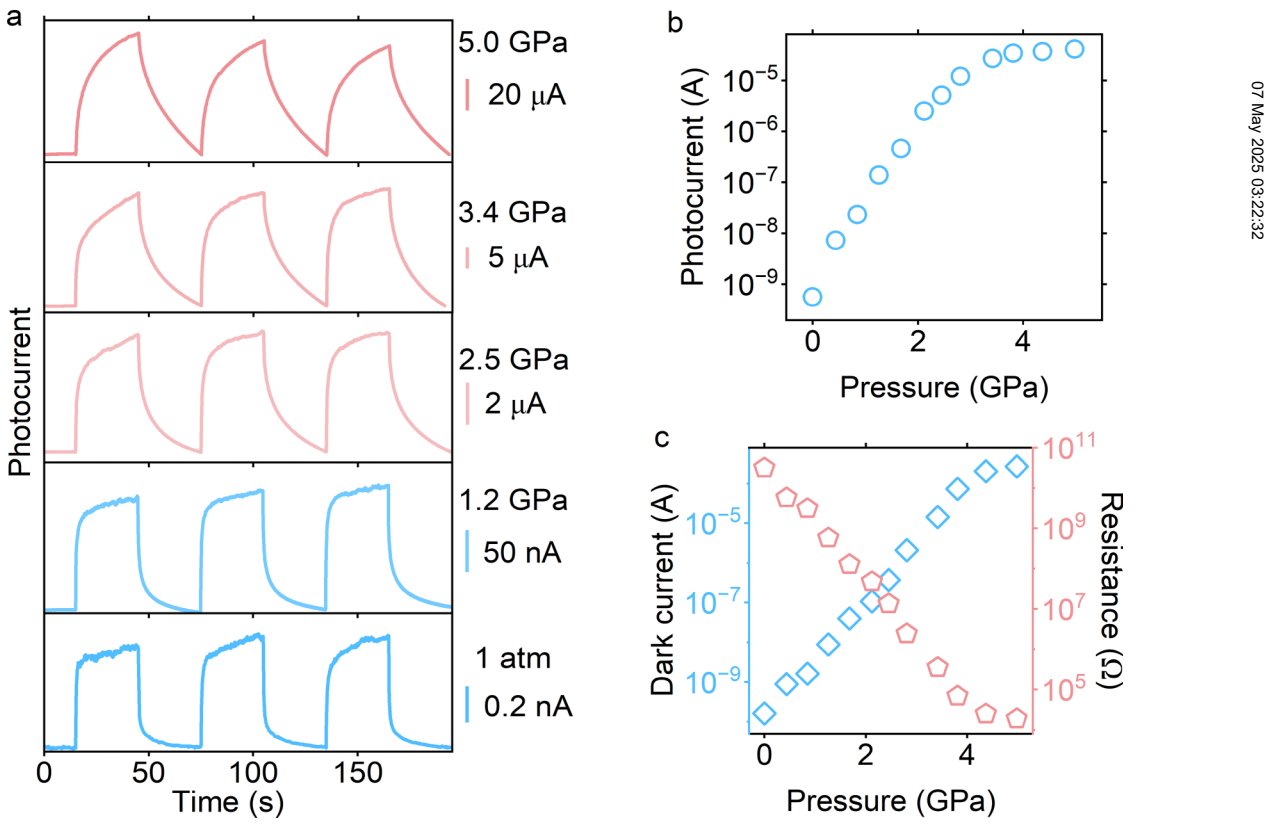

FIG. 6. (a) Time-dependent photocurrent under various pressures. (b) The pressure dependence of photocurrent. (c) Pressure-tuned dark current and resistance of GeI_2.

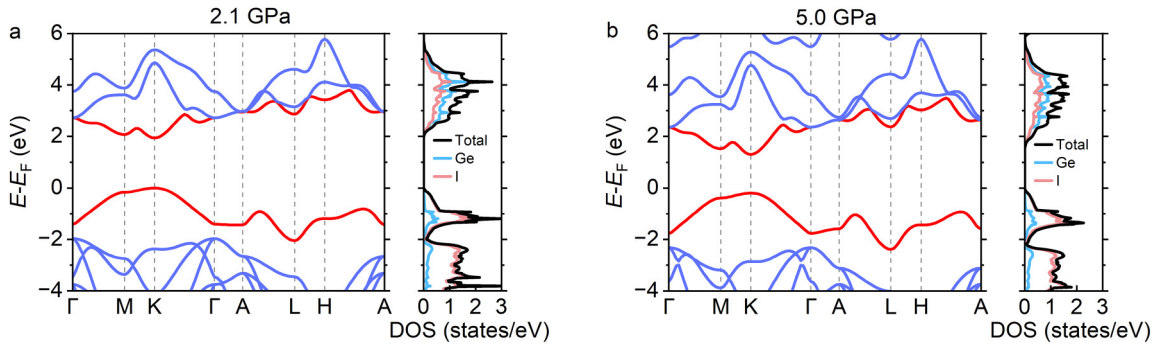

FIG. 7. (a) The calculated band structure and DOS at 2.1 and (b) 5.0 GPa, where the conduction band and valence band are highlighted in red.

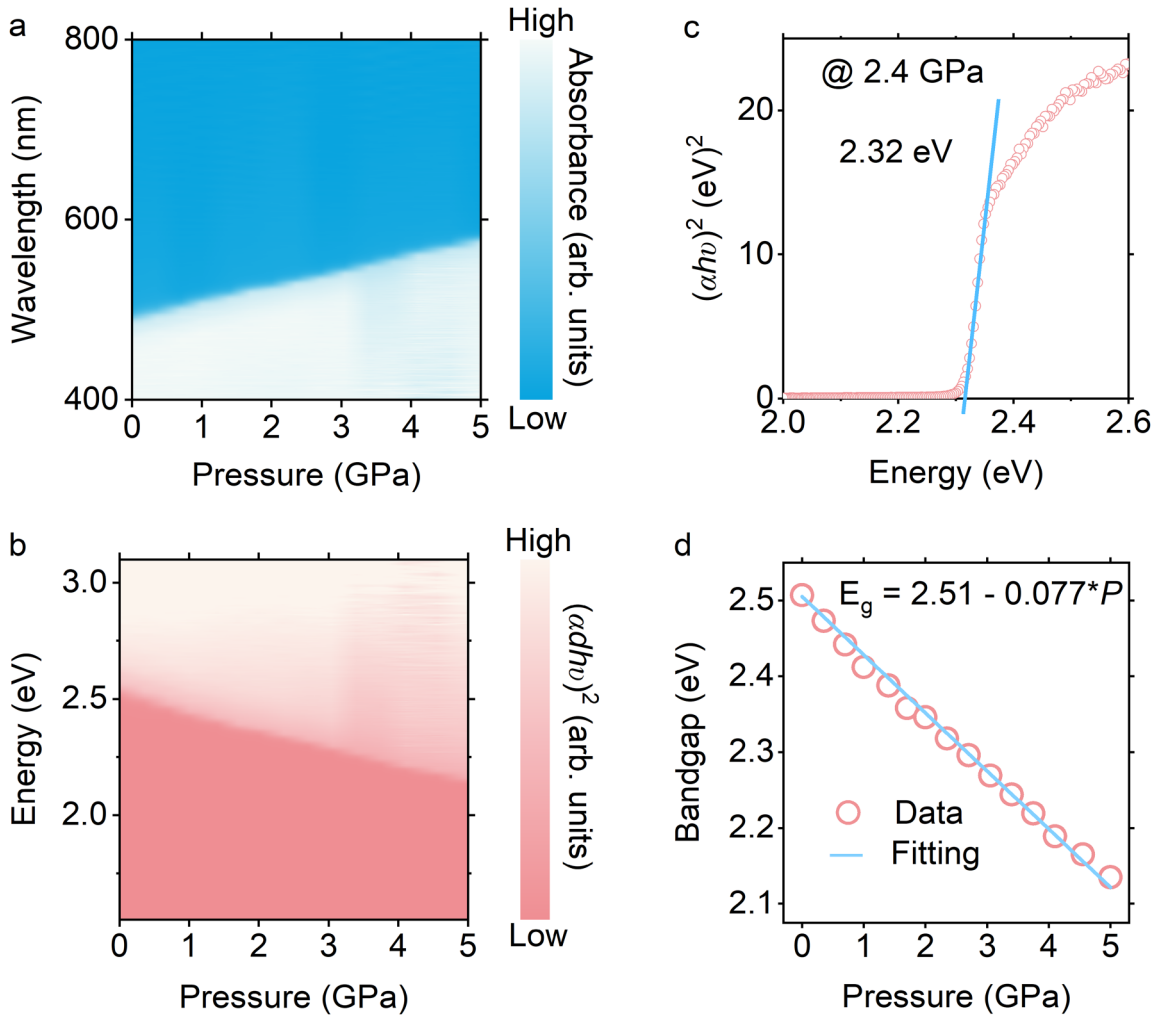

FIG. 8. (a) 2D plot of UV-visible absorption spectroscopy of GeI_2 under pressure. (b) 2D plot of $(\alpha h\nu)^2$ of GeI_2 under compression. (c) Tauc plot for direct bandgap fitting at 2.4 GPa. (d) The pressure-dependent evolution of the bandgap. The solid line represents the linear fitting of the bandgap.

underlying changes in the electronic structure, we performed DFT calculations based on the high-pressure crystal structures obtained from XRD refinements. The calculations were conducted at 2.1 and 5.0 GPa, and the resulting electronic band structures are shown in Figs. 7(a) and 7(b). The results confirm that GeI_2 retains its direct bandgap nature under compression, while the bandgap width decreases consistently with the experimental UV-visible absorption data.

To investigate the pressure-induced changes in the bandgap of GeI_2, we conducted UV-visible absorption spectroscopy under compression. Based on the calculation results, the entire bandgap fitting process maintains a direct bandgap. As shown in Figs. 8(a) and 8(b), the absorption edge shifts systematically toward longer wavelengths with increasing pressure, indicating a continuous narrowing of the bandgap. Based on the calculation results, the bandgap fitting process consistently exhibits a direct bandgap. Figure 8(c) provides an example of the bandgap fitting at 2.4 GPa, demonstrating that the material possesses a direct bandgap of 2.32 eV at this pressure. Based on the Tauc plot fitting, we quantified the bandgap reduction, revealing a nearly linear decrease of 0.077 eV/GPa within the pressure range of 0–5 GPa [Fig. 8(d)]. These results highlight the significant modulation of the electronic structure of GeI_2 by external pressure.

This agreement validates both the experimental and theoretical analyses and underscores the strong influence of pressure on the material's electronic structure. The observed rapid decrease in resistance and the corresponding increase in dark current under pressure, as discussed earlier, can be attributed to the shrinking bandgap. These findings provide a clear link between the pressure-dependent electronic structure of GeI_2 and its optical and electrical behaviors, offering valuable insights for the design of pressure-tunable optoelectronic devices.

III. CONCLUSION

In this work, we synthesized millimeter-scale layered halide compound GeI_2 and investigated its structural, optical, and photoelectric properties under pressures up to 5 GPa. *In situ* Raman spectra and high-pressure XRD measurements revealed that GeI_2 undergoes continuous lattice contraction without undergoing a phase transition. Notably, the dramatic enhancement of photoelectric activity under compression highlights the potential of GeI_2 as a versatile material for wide-spectrum photoresponsive devices, particularly in advanced flexible optoelectronic applications. The observed modulation of the electronic structure, characterized by a significant bandgap reduction, provides critical insight into the pressure-induced changes in the optical and electrical properties of GeI_2. These findings deepen our understanding of the fundamental behaviors of this 2D semiconductor and establish a foundation for its application in the development of innovative optoelectronic devices.

SUPPLEMENTARY MATERIAL

See the supplementary material for specific information about the experimental details and theoretical calculations performed in this article, including SEM and EDS measurements, high-pressure Raman spectra, high-pressure synchrotron XRD, high-pressure absorption spectroscopy, high-pressure photocurrent measurement, GGA-PBE calculations, and HSE calculations.

ACKNOWLEDGMENTS

The authors gratefully acknowledge the financial support provided by the Shanghai Key Laboratory of Material Frontiers Research in Extreme Environments (MFree), China (Grant No. 22dz2260800) and the Shanghai Science and Technology Committee, China (Grant No. 22JC1410300). High-pressure PXRD characterizations were conducted at beamline 15U of the Shanghai Synchrotron Radiation Facility (SSRF). The authors also extend their sincere appreciation to Ms. Yanping Yang (HPSTAR), Dr. Junyue Wang (HPSTAR), Ms. Xueyan Du (HPSTAR), Dr. Lili Zhang (SSRF), and Ms. Huiru Tian (HPSTAR) for their assistance with experimental work.

AUTHOR DECLARATIONS

Conflict of Interest

The authors have no conflicts to disclose.

Author Contributions

Zhongyang Li, Yiming Wang, and Xiaohui Zeng contributed equally to this work.

Zhongyang Li: Data curation (equal); Formal analysis (lead); Writing – original draft (equal). **Yiming Wang:** Data curation (equal); Formal analysis (equal); Writing – original draft (equal). **Xiaohui Zeng:** Data curation (equal); Formal analysis (equal); Writing – original draft (equal). **Shuo Zhou:** Data curation (supporting); Formal analysis (supporting). **Zhikai Zhu:** Data curation (supporting). **Kai Zhang:** Data curation (supporting). **Kejun Bu:** Data curation (supporting). **Chengxuan Song:** Formal analysis (supporting). **Haiyun Shu:** Data curation (supporting). **Shuai Yan:** Data curation (supporting). **Dongbo Wang:** Data curation (supporting). **Wenge Yang:** Writing – review & editing (lead). **Gang Liu:** Data curation (lead); Writing – review & editing (equal). **Yanfeng Guo:** Writing – review & editing (lead). **Lingping Kong:** Data curation (lead); Funding acquisition (lead); Writing – review & editing (lead).

DATA AVAILABILITY

The data that support the findings of this study are available from the corresponding authors upon reasonable request.

REFERENCES

[1]C. He and C. Chen, Photonics **10**, 648 (2023).
[2]D. Zheng and T. Pauporté, Adv. Funct. Mater. **34**, 2311205 (2024).
[3]L. Li, S. Ye, J. Qu, F. Zhou, J. Song, and G. Shen, Small **17**, 2005606 (2021).
[4]W. Wu, H. Lu, X. Han, C. Wang, Z. Xu, S. T. Han, and C. Pan, Small Methods **7**, 2201499 (2023).
[5]H. Y. Kim, J. H. Kim, Y. J. Kim, K. H. Chae, C. N. Whang, J. H. Song, and S. Im, Opt. Mater. **17**, 141–144 (2001).
[6]Y.-G. Zhang, Y. Gu, X.-M. Shao, X. Li, H.-M. Gong, and J.-X. Fang, Chin. Phys. B **27**, 128102 (2018).

[7]M. Casalino, G. Coppola, M. Iodice, I. Rendina, and L. Sirleto, Sensors **10**, 10571–10600 (2010).
[8]X. T. Wang, Y. Cui, T. Li, M. Lei, J. B. Li, and Z. M. Wei, Adv. Opt. Mater. **7**, 1801274 (2019).
[9]X. W. Guan, X. C. Yu, D. Periyanagounder, M. R. Benzigar, J. K. Huang, C. H. Lin, J. Kim, S. Singh, L. Hu, G. Z. Liu, D. H. Li, J. H. He, F. Yan, Q. J. Wang, and T. Wu, Adv. Opt. Mater. **9**, 2001708 (2021).
[10]C. Xie and F. Yan, Small **13**, 1701822 (2017).
[11]S. Krishna, A. Sharma, N. Aggarwal, S. Husale, and G. Gupta, Sol. Energy Mater. Sol. Cells **172**, 376–383 (2017).
[12]M. Long, P. Wang, H. Fang, and W. Hu, Adv. Funct. Mater. **29**, 1803807 (2019).
[13]P. C. Y. Chow and T. Someya, Adv. Mater. **32**, 1902045 (2020).
[14]G. Wang, Y. Zhang, C. You, B. Liu, Y. Yang, H. Li, A. Cui, D. Liu, and H. Yan, Infrared Phys. Technol. **88**, 149–173 (2018).
[15]J. Miao and C. Wang, Nano Res. **14**, 1878–1888 (2021).
[16]T. Mueller, F. Xia, and P. Avouris, Nat. Photonics **4**, 297–301 (2010).
[17]P. Kumbhakar, C. Chowde Gowda, and C. S. Tiwary, Front. Mater. **8**, 721514 (2021).
[18]L. Zheng, X. Wang, H. Jiang, M. Xu, W. Huang, and Z. Liu, Nano Res. **15**, 2413–2432 (2022).
[19]S. Chen, Y. Fu, M. Ishaq, C. Li, D. Ren, Z. Su, X. Qiao, P. Fan, G. Liang, and J. Tang, InfoMat **5**, e12400 (2023).
[20]H. S. Nalwa, RSC Adv. **10**, 30529–30602 (2020).
[21]V. K. Sangwan, D. G. Chica, T.-C. Chu, M. Cheng, M. A. Quintero, S. Hao, C. E. Mead, H. Choi, R. Zu, J. Sheoran, J. He, Y. Liu, E. Qian, C. C. Laing, M.-A. Kang, V. Gopalan, C. Wolverton, V. P. Dravid, L. J. Lauhon, M. C. Hersam, and M. G. Kanatzidis, Sci. Adv. **10**, eado8272 (2024).
[22]Y. Li, J. Fu, X. Mao, C. Chen, H. Liu, M. Gong, and H. Zeng, Nat. Commun. **12**, 5896 (2021).
[23]H.-K. Mao, B. Chen, H. Y. Gou, K. Li, J. Liu, L. Wang, H. Xiao, and W. G. Yang, Matter Radiat. Extr. **6**, 013001 (2021).
[24]L. P. Kong, J. Gong, Q. Y. Hu, F. Capitani, A. Celeste, T. Hattori, A. Sano-Furukawa, N. N. Li, W. G. Yang, G. Liu, and H.-K. Mao, Adv. Funct. Mater. **31**, 2009131 (2021).
[25]L. P. Kong, J. Gong, I. Spanopoulos, S. Yan, Z. Y. Li, Z. Z. Zhu, X. Y. Liu, Y. N. Zhu, H. L. Dong, H. Y. Shu, Q. Y. Hu, W. G. Yang, H.-K. Mao, M. G. Kanatzidis, and G. Liu, Adv. Funct. Mater. **34**, 2414437 (2024).
[26]S. H. Guo, K. J. Bu, J. W. Li, Q. Y. Hu, H. Luo, Y. H. He, Y. H. Wu, D. Z. Zhang, Y. S. Zhao, W. G. Yang, M. G. Kanatzidis, and X. J. Lü, J. Am. Chem. Soc. **143**, 2545 (2021).
[27]Z. L. Li, Q. J. Li, H. Y. Li, F. Y. Tian, M. Y. Du, S. X. Fang, R. Liu, L. J. Zhang, and B. B. Liu, Small Methods **6**, 2201044 (2022).
[28]Z. L. Li, Q. J. Li, H. Y. Li, L. Yue, D. L. Zhao, F. Y. Tian, Q. Dong, X. T. Zhang, X. L. Jin, L. J. Zhang, R. Liu, and B. B. Liu, Adv. Funct. Mater. **32**, 2108636 (2022).
[29]Y. Q. Fang, L. P. Kong, R. Q. Wang, Z. Zhang, Z. Y. Li, Y. H. Wu, K. J. Bu, X. Q. Liu, S. Yan, T. Hattori, N. A. Li, K. Li, G. Liu, and F. Q. Huang, Mater. Today Phys. **34**, 101083 (2023).
[30]G. R. Hou, N. Antonatos, K. J. Sarkar, L. P. Liao, B. Wu, J. Luxa, V. Mazánek, L. Děkanovský, D. Sedmidubský, A. P. Herman, R. Kudrawiec, and Z. Sofer, ACS Appl. Electron. Mater. **5**, 4401–4408 (2023).
[31]C. Prescher and V. B. Prakapenka, High Pressure Res. **35**, 223 (2015).
[32]B. H. Toby and R. B. Von Dreele, J. Appl. Crystallogr. **46**, 544 (2013).
[33]Z. Y. Li, X. H. Zeng, K. J. Bu, Z. K. Zhu, Y. M. Wang, J. Yuan, X. F. Hou, H. Y. Shu, S. Yan, W. G. Yang, L. P. Kong, G. Liu, and Y. F. Guo, Appl. Phys. Lett. **125**, 061103 (2024).
[34]L. Yue, D. D. Cui, F. B. Tian, S. Liu, Z. L. Li, R. Liu, Z. Yao, Y. C. Li, D. L. Yang, X. D. Li, Q. J. Li, Y. Du, and B. B. Liu, Acta Mater. **263**, 119529 (2024).
[35]K. J. Bu, T. H. Fu, Z. W. Du, X. Feng, D. Wang, Z. Y. Li, S. H. Guo, Z. D. Sun, H. Luo, G. Liu, Y. Ding, T. Y. Zhai, Q. Li, and X. J. Lü, Chem. Mater. **35**, 242–250 (2023).
[36]L. Zhang, L. W. Wu, K. Wang, and B. Zou, Adv. Sci. **6**, 1801628 (2019).
[37]T. Katsura and Y. Tange, Minerals **9**, 745 (2019).